Numerical Investigation of the Drag of Twin Prolate Spheroid Hulls in Various Longitudinal and Transverse Configurations

Pareecha Rattanasiri*, Philip A. Wilson† and Alexander B. Phillips‡
Faculty of Engineering and the Environment
University of Southampton
Southampton, United Kingdon SO17 1BJ
Email: *pj506@soton.ac.uk, †philip.wilson@soton.ac.uk
and ‡abp@soton.ac.uk

***Abstract*—The purpose of this paper is to provide guidance for operators on suitable spacings for multiple vehicle missions. This paper then investigates the combined drag of a pair of towed prolate spheroids for the length-Reynolds Number of 3.2×10^6. The model has a length-diameter ratio of 6:1. A series of configuration of a pair of spheroids is simulated by varying both longitudinal and transverse spacing. Three-dimensional simulations are performed using a commercial Reynolds Averaged Navier Stokes (RANS) Computational Fluid Dynamics code ANSYS CFX 12.1 with the SST turbulence closure model. In each case, the fluid domain has a mesh size of approximately nine million cells including inflated prism layers to capture the boundary layer. Mesh convergence is tested and then validated with wind tunnel test results. The drag of each spheroid is compared against the benchmark drag of a single hull.**

The results show that the transverse separations and longitudinal offsets determine the interaction drag between both hulls. Increasing of spacing results in lower the interference drag. Five zones have been suggested based on the characteristics of the combined drag and individual drags. These are Parallel Region, Echelon Region, Low Interaction Region, Push Region and Drafting Region. Based on the results, operators can determine the optimal configurations based on energy considerations.

I. Introduction

Autonomous Underwater Vehicles (AUVs) are self-propelled systems which perform missions without requiring external powering or umbilical control. Proposed missions for the next generation of AUVs require high quantity and quality temporal and spatial data which will nessecatate multiple AUVs [1], [2]. This has led to the investigation of manoeuvering and path planning of fleets of AUVs [3]–[10]. By carrying different sensors, the surveying performance of multiple small AUVs may be equal or exceed that of a single larger vehicle, with improved levels of robustness and redundancy.

Observation of animal motion such as fish in schools, dolphins in pods or birds in flocks suggest some energetic performance benefit may be obtained by certain fleet configurations [11]–[16]. These results lead to the underlying questions of:-

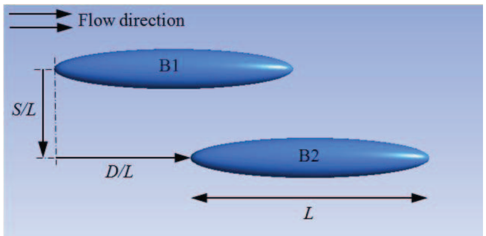

Fig. 1: A pair of prolate spheroids

TABLE I: Test Matrix

$S/L \setminus D/L$	0.27	0.57	0.87	1.17	1.47
0.17	✓	✓	✓	✓	✓
0.27	✓	✓	✓	✓	✓
0.37	✓	✓	✓	✓	✓
0.47	✓	✓	✓	✓	✓

- does a fleet configuration energy benefits just an individual AUV or the whole fleet?
- what is the optimal configuration of the fleet?

In 1997, Molland and Utama [17] performed a series of experiments to investigate the drag characteristics of a pair of prolate spheroids at a Reynolds Number (Re) of $3.2{\times}10^6$. The length (L) of each spheroid was 1.2 m with a length-diameter ratio of 6:1. The wetted surface area is 0.601 m^2. By varying transverse separation (S/L) at zero longitudinal offset ($D/L = 0$), the results show that the presence of a second spheroid (B2) changed the magnitude of forces acting on the reference spheroid (B1). For S/L of 0.27, 0.37 and 0.47, the drag coefficient based on wetted surface area of B1 ($C_{D(B1)}$) is 8%, 4% and 2% higher than that of single hull ($C_{D(s)}$), respectively. See Fig. 1 for configuration's spacing reference.

Recently the investigation of multiple torpedo shape AUVs using CFD simulation was published by Husaini [18]. The simulation shows that the arrangement and spacing between B1 and B2 influences the drag on both hulls.

This paper extends numerically the experiments of Molland and Utama to consider both longitudinal and transverse spacing, detail shown in Table I. The purpose of these simulations is to provide guidance for operators on suitable spacing for multiple vehicle missions.

II. Numerical Method

Prediction of the hydrodynamic forces acting on an AUV's hull can be modelled using steady-state Reynolds Averaged Navier Stokes (RANS) simulations. This has proved to provide reasonably accurate results with modest computational cost [19]–[23]. Thus a RANS approach is chosen to perform the drag prediction in this numerical experiment.

By assuming the flow is incompressible, the continuity equation becomes:-

$$\frac{\partial \overline{U_i}}{\partial x_i} = 0 \tag{1}$$

The momentum equation can be written as:-

$$\rho\left(\frac{\partial \overline{U_i}}{\partial t} + \frac{\partial \overline{U_i U_j}}{\partial x_j}\right) = -\frac{\partial P}{\partial x_i} + \frac{\partial}{\partial x_j}\left\{\mu\left(\frac{\partial \overline{U_i}}{\partial x_j} + \frac{\partial \overline{U_j}}{\partial x_i}\right)\right\} - \rho\frac{\partial \overline{u_i' u_j'}}{\partial x_j} + f_i \tag{2}$$

where the tensor x_i represents Cartesian co-ordinates (X, Y, Z) and u_i are the Cartesian mean velocity components ($\overline{U_x}$, $\overline{U_y}$, $\overline{U_z}$). The Reynolds stress tensor ($\overline{\rho u_i' u_j'}$) is represented the turbulence closure. The Shear Stress Transport (SST) model, which blends $k-\epsilon$ and $k-\omega$, was proved to provide a good result for a moderated run time [23]. Therefore the SST model is selected as a turbulence model.

CFD Simulation has been set up as following:-

Model Domain: To compare results with [17], The dimension of fluid domain, $1.4L \times 12L \times 1.8L$, is modelled to replicate wind tunnel boundary.

Boundary Conditions: To replicate the experimental conditions, the model domain is set up by using zero relative pressure at outlet. Free-slip walls are used for roof, floor and walls. The air inlet velocity is set at 40 m/s related to a Re of 3.2×10^6. The air density (ρ_{air}) and the air kinematic viscosity (υ_{air}) at room temperature are 1.185 kg/m^3 and 1.545×10^{-5} m^2/s, respectively. The hulls' are modelled by using no-slip wall condition. Fig. 2 illustrates the model domain and boundary condition used in this simulation.

Mesh Strategy: Fig. 3 and 4 shows the meshes in three-dimensional fluid domain. A series of 8 meshes ranging from 1.2-25M elements were made for an exampler case. Based on this study, mesh parameters of global mesh size and local refinement around hulls in X, Y and Z direction where selected as appropriate

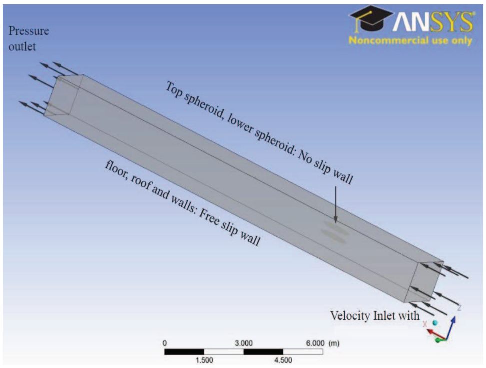

Fig. 2: Boundary condition of a pair of prolate spheroids in the three-dimensional fluid domain

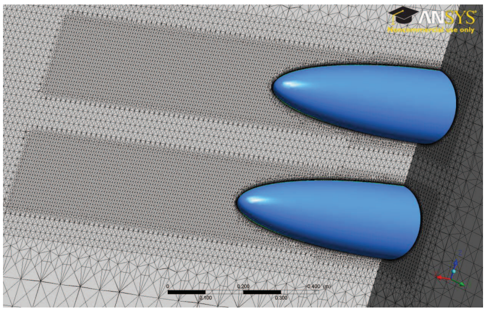

Fig. 3: Three-dimensional elements around tail of a pair of spheroids for S/L = 0.27 and D/L = 0

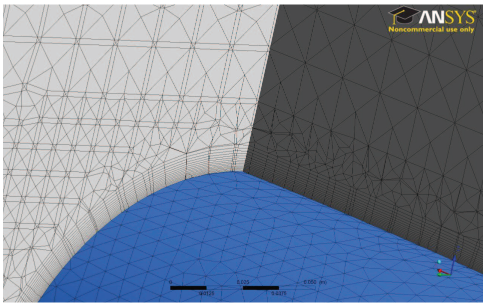

Fig. 4: Three-dimensional inflated prisms 15 layers

TABLE II: Computaional Parameters

Parameters	Setting
Mesh type	Unstructured with local refinement around spheroids and in wake regions
No. of elements	approximately 8-15M
y^+	30 with 15 layers in the boundary layer
Turbulence model	Shear Stress Transport
Inlet turbulent intensity	1%
Wall modelling	Automatic Wall Function [24]
Spatial discretisation	High Resolution [24]
Timescale control	Auto Timescale [24]
Convergence criteria	RMS residual $< 10^{-6}$
Computing	Iridis 3 Linux Cluster
Run type	Parallel (12 partitions run on 4×Dual core nodes, each with 2GB RAM)
Simulation Time	2.0-2.5 hours

resulting meshes for the various configurations have 8-15M elements with $y^+ = 30$ and 15 elements in boundary layer.

Detail of the computational parameters is provided in Table II.

III. Validation

The results illustrate the impact of flow interaction over both hulls. Comparisons are made with the experimental results [17], previous numerical results [25] and empirical results [26] are as following.

A. Pressure distribution

Fig. 5 shows the distribution of pressure coefficient, $C_P = \frac{P-P_\infty}{0.5\rho U^2}$. Where X is a position on the longitudinal axis of the body.

For three separated studies, good agreement is observed between numerical and experimental results.

B. Sideforce coefficient

Sideforce is defined as attraction between hulls and Sideforce coefficient (C_{SF}) is defined as $\frac{F_z}{0.5\rho U^2}$. In Fig. 6, the numerical results of C_{SF} of B1 show a good agreement with experimental results. The rapid decreasing of sideforce ratio with increasing of separation is due to lower flow velocity through contruction between the hulls.

C. Form factor

A form factor $(1+k)$ was introduced to estimate the ratio of total viscous drag to skin friction drag (C_v/C_F) as:-

$$C_v = (1+k)C_F \tag{3}$$

As the early state of drag prediction, the ITTC'57 correction line [27] is commonly used to estimate the C_F as a function of Re:-

$$(C_F)_{1957} = \frac{0.075}{\left(log_{10}\ (Re) - 2\right)^2} \tag{4}$$

For streamlined shapes, Hoerner [26] suggests a form factor may be estimated in term of body length (L) and maximum body diameter (d_m) as:-

$$(1+k) = 1 + 1.5(d_m/L)^{3/2} + 7(d_m/L)^3 \tag{5}$$

By assuming that the AUV is fully submerged in deep water, the total drag can be estimated as:-

$$C_D = C_v = (1+k)C_F \tag{6}$$

In the case of twin hulls, the conventional form factor cannot establish accurate prediction due to the presence of viscous interaction between hulls. By combining a viscous resistance factor β, the estimation of a more accurate form factor (1+βk) can be obtained [25], hence the total drag of twin hulls can be estimated as:-

$$C_D = C_v = (1+\beta k)C_F \tag{7}$$

The comparison of form factor between experimental and numerical results based on the ITTC correction line is shown in Fig. 7. For the length-diameter ratio 6:1 spheroid, estimated $(1+k)$ of each spheroid from Equation 5 should be 1.135. The numerically predicted $(1+k)$ of B1 is within 1.5% error of the Hoerner's estimation. Whilst the experimental predicted $(1+k)$ is 8% error compared to the Hoerner's.

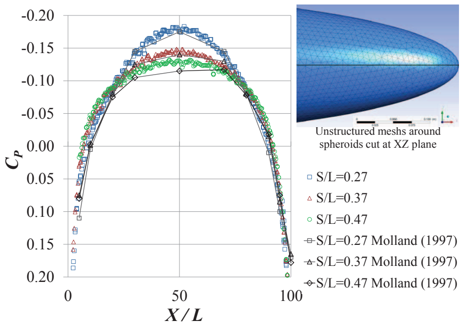

Fig. 5: C_P along X/L of the inner side surface of B1 (perpendicular to B2)

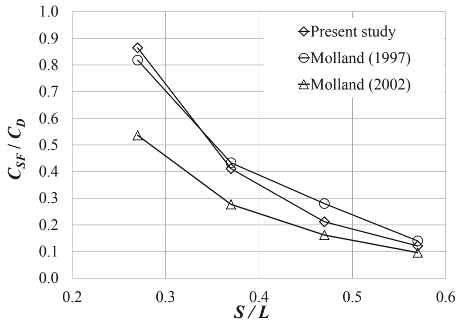

Fig. 6: C_{SF} as proportion of C_D

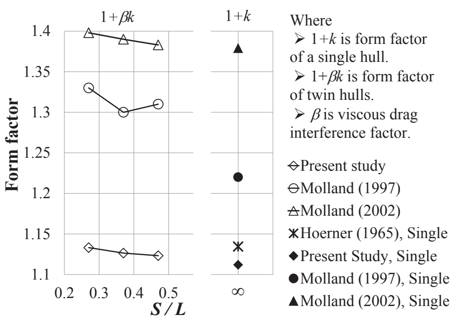

Fig. 7: Form factor

IV. Impact of Fleet Configuration on Drag

The results are discussed in terms of the three-dimensional total drag coefficient based on wetted surface area (C_D), the pressure drag coefficient (C_{Px}) and the skin friction drag coefficient (C_F),

$$\begin{aligned} C_D &= (\text{Total drag})/0.5\,\rho\,V^2 A_w \\ C_{Px} &= (\text{Pressure drag})_x/0.5\,\rho\,V^2 A_w \\ C_F &= (\text{Skin friction drag})/0.5\,\rho\,V^2 A_w \end{aligned} \quad (8)$$

where V is the fluid flow velocity.

Results are presented for various configurations in Fig. 8. $\%B1$ and $\%B2$ is the percentage difference of the individual drag of B1 and B2 referred to a single hull, respectively. Whilst $\%CB$ is the percentage difference of combined drag referred to twice that of a single hull,

$$\begin{aligned} \%B1 &= \frac{C_{D(B1)}-C_{D(s)}}{C_{D(s)}} \times 100 \\ \%B2 &= \frac{C_{D(B2)}-C_{D(s)}}{C_{D(s)}} \times 100 \\ \%CB &= \frac{C_{D(B1)}+C_{D(B2)}-2C_{D(s)}}{2C_{D(s)}} \times 100 \end{aligned} \quad (9)$$

where $C_{D(B1)}$ and $C_{D(B2)}$ is the drag coefficient of B1 and B2, respectively. $C_{D(s)}$ is drag coefficient of a single hull.

The results suggest some energetically beneficial configurations, both for individuals and the whole fleet. However, some configurations lead to significant increases in hull drag. The results may be classified into five regions (See Table III).

TABLE III: Map of Twin Hulls' Drags

Name	S/L	D/L
Parallel Region	0.17-0.47	0
Echelon Region	0.17-0.27	0.27-0.57
	0.37-0.47	0.27-0.87
Low Interaction Region	0.17	≥1.47
	0.27	≥0.87
	0.37-0.47	≥1.17
Push Region	0.17	0.87-1.17
	0	<1.37
Drafting Region	0	>1.37

A. Parallel region

With both hulls parallel to the inflow, noses aligned without any longitudinal offset, both hulls experience an equal interference drag, due to accelerated flow passing between them. The results show that as the transverse separation (S/L) is extended from 0.17 to 0.47, individual and combined drag decreases by 10% to 2%.

The results plot in Fig. 9(a), 9(c) and 9(e) suggest that the drag penalty in this region caused by an increment on both pressure drag and skin friction.

B. Echelon region

With any transverse separation and limitation of longitudinal offset within one body length, the configuration is similar to echelon or 'vee' formation of birds (the followers fly in symmetrical V-Shape after a leader). The drag penalty of combined drag can reach up to approximately 7% when the nose of B2 placed close to nose of B1.

As B2 is moved backward, the combined drag is reduced. Likewise, increasing the transverse separation causes the combined drag to decrease. The individual drags indicate the substantial drags' interchange. It appears that B2 pushes an extra penalty to B1 for its own advantage. For example, at $S/L = 0.17$ and $D/L = 0.27$, B2 has 94% of drag reduction, whilst drag of B1 is twice of that of a single hull.

From Fig. 9(a), 9(c) and 9(e), it suggests that within one body length of the longitudinal offset, the changes of C_D are dominated by the changes of pressure drag rather than the minimal change of skin friction.

The diverse trend of drag's interaction between two hulls roughly begins at 0.70 longitudinal offset ($D/L = 0.70$), B1 gains some benefit from a fleet whilst B2 gets the drag penalty. However, the magnitude of all drags is relatively small compared to that of 0.17-0.70 longitudinal offset ($0.17 < D/L < 0.70$).

C. Low Interaction Region

Configuration of Low Interaction Region is a spacing combination of any transverse separation with more than 1.17 longitudinal offset ($D/L > 1.17$). The combined drag shows a minimal change, less than 1% of drag reduction. It also suggests the larger spacing between two hulls results in less forces' interaction between them. Individually, the B2 gets a drag penalty whilst B1 gains some benefit. However, on average, the individual drag exchange is less than 2%.

From Fig. 9(a), 9(c) and 9(e), the trend of drags follows that of Echelon Region with the small magnitude of reduction in comparison.

figure

D. Push region

Push Region is where the nose of B2 is positioned close to the trailing edge of B1. The combined drag can be reduced by 1%-7% and B1 experiences a moderate reduction in drag due to pressure of B2.

At $S/L = 0$, drag of B1 is reduced by 20% whilst drag of B2 is increased by 7%. At $S/L = 0.17$, B1 gains 16% reduction from the configuration by trading a 13% drag penalty to B2. Typically, because of the B2 is pushing B1 forward. As the stagnation of flow of B2 interferes at the rear part of B1, consequently, the pressure drag of B1 is reduced.

S/L \ D/L	D/L = 0	0.27	0.57	0.87	1.17	1.47	1.77
					Push Region	Drafting Region	
S/L = 0	%B1 / %B2 %CB				-20.8 / 6.9 -7.0	-4.0 / -7.4 -5.7	-1.3 / -8.0 -4.6
0.17	10.0 / 9.8 9.9	107.3 / -93.9 6.7	64.0 / -62.4 0.8	-15.8 / 12.8 -1.5	-11.9 / 10.3 -0.8	-3.2 / 2.5 -0.4	-0.9 / 0.3 -0.3
0.27	4.4 / 4.7 4.6	55.6 / -49.7 3.0	38.1 / -37.3 0.4	-2.2 / 0.7 -0.7	-6.4 / 5.4 -0.5	-2.1 / 1.6 -0.3	-0.6 / 0.2 -0.2
0.37	3.0 / 2.8 2.9	33.0 / -28.7 2.2	26.0 / -25.1 0.5	3.5 / -4.1 -0.3	-2.5 / 1.7 -0.4	-1.0 / 0.5 -0.3	-0.3 / -0.2 -0.2
0.47	2.4 / 2.2 2.3	21.1 / -17.8 1.6	19.1 / -17.7 0.7	5.7 / -5.8 -0.1	0.0 / -0.5 -0.2	-0.2 / 0.0 -0.1	-0.1 / -0.2 -0.2
	Parallel Region	Echelon Region			Low Interaction Region		

Fig. 8: The percentage difference of C_D comparing to a single hull for $Re = 3.2 \times 10^6$, $+$ and $-$ indicates increasing and decreasing of drags, respectively.

Fig. 9(b), 9(d) and 9(f) intensively shows the drag change at various longitudinal spacing ($1.17 \leq D/L \leq 4.47$) in zero separation configuration ($S/L = 0$). Within $0.5L$, Fig. 9(f) shows no change of skin friction for B1 and a moderate reduction of the skin friction for B2. In Fig. 9(d), the C_{Px} of B1 is significantly dropped almost 100%, whilst C_{Px} of B2 increases up to 250% at $D/L = 1.17$. These results suggest the insignificant change of skin friction in this region.

E. Drafting Region

By placing B2 directly behind B1 at $D/L > 1.37$, this region is termed Drafting Region and is identical to slipstreaming in cycling and swimming [28]–[30]. The combined drag can be reduced by 5%-6% with individual drag reduction by 7%-8% for B2 and 2%-4% for B1.

By considering Fig. 9(b), 9(d) and 9(f), as longitudinal offset increases, the results suggest a loss of energy benefit. Typically, because of the attached flow is predominant. At $D/L \geq 5$, the drag reduction for B2 is trending towards free stream drag value as wake recovery occurs.
figure

V. Discussion

Overall, the transverse separations and longitudinal offsets determine the interference drag between both hulls. Increasing of spacing results in lower interactions.

The Parallel Region, the smaller the spacing, the larger the drag penalty caused by viscous interactions. These characteristics had also been observed by Molland and Utama [25]. It can be assumed that to avoid interaction drag, transverse separation of both hulls must be at least $0.5L$.

The Echelon Region can be used to explain the neonate and infant position of dolphin calfs. The calf will swim as close to its mother as possible with nose almost touch its mother's abdomen [15], [16]. The Echelon configuration could potentially be used to lower propulsion cost of an individual in the fleet.

Applications where close proximity is required, the Low Interaction Region can be indicated as the minimum spacing of configurations.

In these simulations, the drafting region provides the optimum configuration to minimise fleet drag. However, most AUVs are propeller driven; therefore, our studies in the Drafting configuration are limited. Since the action of the propeller will re-energise the wake region, potentially reducing/removing the observed benefits.

VI. Conclusion

To study the energy impact of fleet configurations, CFD simulations of a pair of equal sized prolate spheroids has been performed at $Re = 3.2 \times 10^6$. Results validated have been agreed with Ref. [17], [25] and [26], the results is then analysed with a degree of confidence.

Five zones have been identified based on the characteristics of the combined drag and individual drags. These are Parallel Region, Echelon Region, Low Interaction Region, Push Region and Drafting Region. Based on the results, operators can determine a potential fleet based on energy considerations.

For further study, it is possible to use different sized spheroids to save energy, such as bigger sized for leader and smaller sized for follower Echelon configuration. The identical configuration to swimming of mother-calf dolphin suggests an improvement of energy benefit.

Furthermore, the propeller's wake region has been excluded from the simulation, the investigation by modelling a propeller's source will provide more information.

Acknowledgment

The authors acknowledge the use of the IRIDIS High Performance Computing Facility, and associated support services at the University of Southampton, in the completion of this work.

The work presented in this paper was financed by the Royal Thai Government.

References

[1] D. Edwards, T. Bean, D. Odell, and M. Anderson, "A leader-follower algorithm for multiple AUV formations." in *In Proceedings of IEEE/OES Autonomous Underwater Vehicles, vol. 1 Sebasco, ME*, 2004, pp. 40–46.

[2] S. Botelho, R. Neves, and L. Taddei, "Localization of a fleet of AUVs using visual maps," *Oceans 2005 - Europe*, vol. 2, pp. 1320–1325, 2005.

[3] A. Martins, J. M. Almeida, and E. Silva, "Coordinated maneuver for gradient search using multiple AUVs," *OCEANS 2003. Proceedings*, vol. 1, pp. 247–352, 2003.

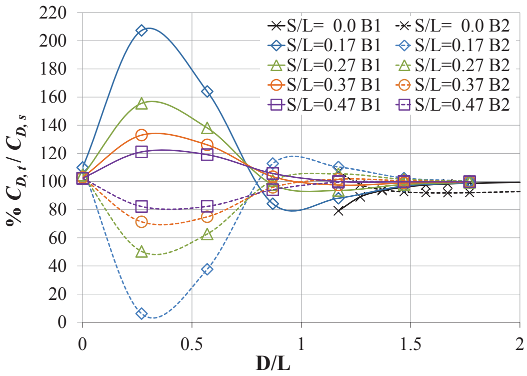

((a)) $\%C_{D,t}/C_{D,s}$

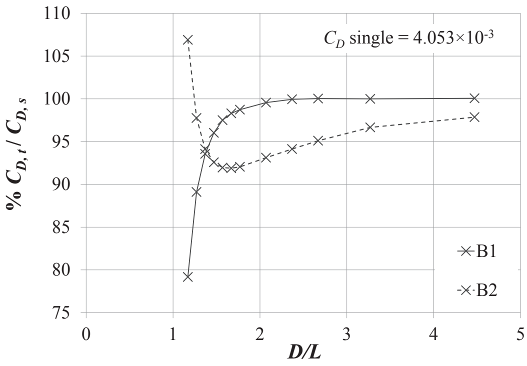

((b)) $\%C_{D,t}/C_{D,s}$ at $S/L = 0$

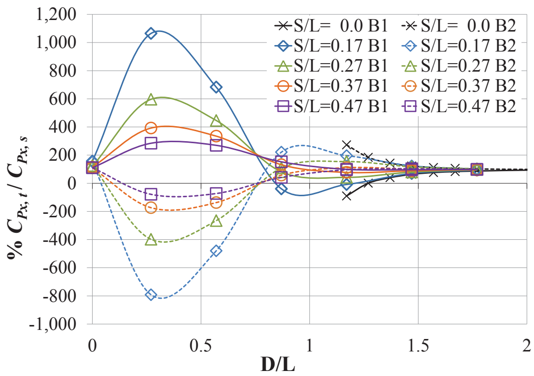

((c)) $\%C_{Px,t}/C_{Px,s}$

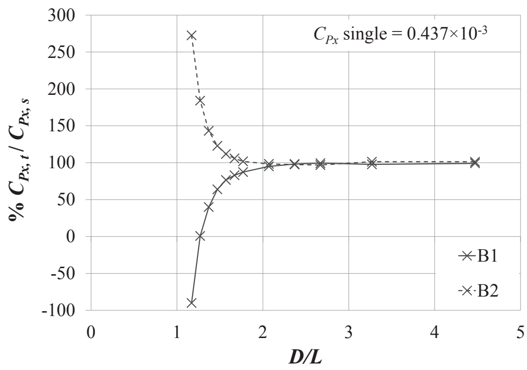

((d)) $\%C_{Px,t}/C_{Px,s}$ at $S/L = 0$

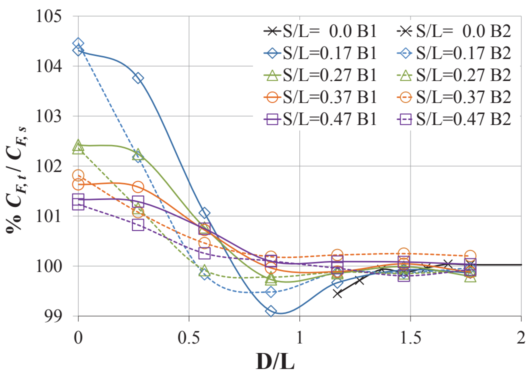

((e)) $\%C_{F,t}/C_{F,s}$

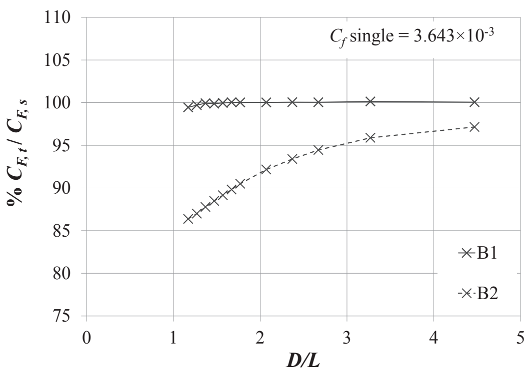

((f)) $\%C_{F,t}/C_{F,s}$ at $S/L = 0$

Fig. 9: Drags' characteristics

[4] C. A. Reeder, D. L. Odell, A. Okamoto, M. J. Anderson, and D. B. Edwards, “Two-hydrophone heading and range sensor applied to formation-flying for AUVs,” in *OCEANS ’04. MTTS/IEEE TECHNO-OCEAN ’04*, 2004, pp. 517–523.

[5] F. V. Vanni, “Coordinated motion control of multiple autonomous under vehicle,” Master’s thesis, Technical University of Lisbon, 2007.

[6] T. Bean, G. Beidler, J. Canning, D. Odell, R. Wall, M. ORourke, D. Edwards, and M. Anderson, “AUV cooperative operations using acoustic communication and navigation,” *IEEE Journal of Oceanic Engineering*, 2007.

[7] R. Cui, S. S. Ge, B. V. E. How, and Y. S. Choo, “Leader-follwer formation control of underactuated AUVs with leader position measurement.” in *Proceedings of the 2009 IEEE International Conference on Robotics and Automation, Kobe, Japan*, 2009, pp. 2441–2446.

[8] M. Burger, A. Pavlov, and K. Pettersen, “Conditional integrators for path following and formation control of marine vessels under constant disturbances,” in *The 8th IFAC International Conference on Manoeuvring and Control of Marine Craft*, Sept 2009, pp. 179–184.

[9] R. Cui, S. S. Ge, B. V. E. How, and Y. S. Choo, “Leader-follwer formation control of underactuated AUVs.” *Ocean Engineering*, pp. 1491–1502, 2010.

[10] A. P. Aguiar, J. Almeida, M. Bayat, B. Cardeira, R. Cunha, A. Hausler, P. Maurya, A. Oliveira, A. Pascoal, A. Pereira, M. Rufino, L. Sebastiao, C. Silvestre, and F. Vanni, “Cooperative control of multiple marine vehicles: Theoretical challenges and practical issues,” *Control & Automation (MED), 2011 19th Mediterranean Conference on*, pp. 424–429, 2011.

[11] B. L. Partridge, J. Johansson, and J. Kalish, “The structure of schools of giant bluefin tuna in cape cad bay,” *Environmental Biology of Fishes*, vol. 9, pp. 253–262, 1983.

[12] B. Hanrahan and F. Juanes, “Estimating the number of fish in atlantic bluefin tuna schools using models derived from captive school observations,” *Fishery Bulletin*, vol. 99(3), 2001.

[13] M. Andersson and J. Wallander, “Kin selection and reciprocity in flight formation?” *Behavioral Ecology*, vol. 15, no. 1, pp. 158–162, 2003.

[14] R. M. Alexander, “Hitching a lift hydrodynamically - in swimming, flying and cycling,” *Journal of Biology*, vol. 3, 2004.

[15] D. Weihs, “The hydrodynamics of dolphin drafting,” *Journal of Biology*, vol. 3:8, 2004.

[16] D. Weihs, M. Ringel, and M. Victor, “Aerodynamic interactions between adjacent slender bodies instrumentation and wind tunnel testing,” *Instrumentation in Aerospace Simulation Facilities, 2007. ICIASF 2007. 22nd International Congress on*, pp. 1–28, 2007.

[17] A. F. Molland and I. K. A. P. Utama, “Wind tunnel investigation of a pair of ellipsoids in close proximity,” Ship Science, University of Southampton, Tech. Rep. 98, 1997.

[18] M. Husaini, Z. Samad, and M. R. Arshad, “CFD simulation cooperative AUV motion,” *Indian Journal of marine Sciences*, vol. 38(3), pp. 346–351, 2009.

[19] T. Sarkar, P. G. Sayer, and S. M. Fraser, “A study of autonomous underwater vehicle hull forms using computational fluid dynamics,” *International journal for Numerical Methods in Fluids*, vol. 25, pp. 1301–1313, 1997.

[20] A. B. Phillips, M. Furlong, and S. R. Turnock, “The use of computational fluid dynamics to assess the hull resistance of concept autonomous underwater vehicles,” in *In, OCEANS 2007 - Europe. Richardson TX, USA, Institute of Electrical and Electronics Engineers*, 2007.

[21] P. Jagadeesh, M. Murali, and V. G. Idichandy, “Experimental investigation of hydrodynamic force coefficients over AUV hull form,” *Journal of Ocean Engineering*, vol. 36, pp. 113–118, 2009.

[22] M. M. Karim, M. M. Rahman, and M. A. Alim, “Computation of turbulent viscous flow around submarine hull using unstructured grid,” 2009.

[23] A. B. Phillips, “Cost effective hydrodynamic concept design of autonomous underwater vehicle.” Ph.D. dissertation, School of Engineering Sciences, 2009.

[24] ANSYS, *ANSYS CFX, Release 12.1*, ANSYS, 2010.

[25] A. F. Molland and I. K. A. P. Utama, “Experimental and numerical investigations of a pair a ellipsoids in close proximity,” in *In Proceedings of the Institution of Mechanical engineers, Part M: Journal of Engineering for the Maritime Environment*, 2002.

[26] S. F. Hoerner, *Fluid-dynamic drag: practical information on aerodynamic drag and hydrodynamic resistance*. (pubished by the author), 1965.

[27] ITTC, “Proceedings of the 8th ittc, madrid, spain.” in *Canal de Experiencias Hidrodinamicas, El Pardo, Madrid*, 1957.

[28] C. R. Kyle, “Reduction of wind resistance and power output of recing cyclists and runners traveling in group,” *Ergonomics*, vol. 22, pp. 387–397, 1979.

[29] S. D. McCole, K. Claney, J. C. Conte, R. Anderson, and J. M. Hagberg, “Energy expenditure during bicycling,” *Journal of Applied Physiology*, vol. 68, pp. 748–753, 1990.

[30] A. J. Silva, A. Rouboa, A. Moreira, V. M. Reis, F. Alves, J. P. Vilas-Boas, and D. A. Marinho, “Analysis of drafting effects in swimming using computational fluid dynamics,” *Journal of Sports Science and Medicine*, vol. 7, pp. 60–66, 2008.